

SPECTROSCOPY OF COLLECTIVE MODES IN A BOSE-EINSTEIN CONDENSATE: FROM SINGLE TO DOUBLE ZONES OF EXCITATIONS

L. A. Machado ^{1*}, L. Madeira ¹, M. A. Caracanhas ¹, and V. S. Bagnato ^{1,2,3}

¹Instituto de Física de São Carlos, Universidade de São Paulo, CP 369, 13560-970 São Carlos, Brazil

²Department of Biomedical Engineering, Texas A&M University, College Station, Texas 77843, USA

³Department of Physics & Astronomy, Texas A&M University, College Station, Texas 77843, USA

ABSTRACT

Collective modes are coherent excitations in Bose-Einstein condensates (BECs), and their study provides insight into the macroscopic quantum phenomena that govern these systems. Collective mode frequencies can be used to probe the properties of BECs, such as the trap geometry, the interatomic interactions, and the presence of defects; hence, it is essential to develop methods for high-resolution determination of collective mode frequencies. A standard technique consists of a single pulse of an external oscillatory field, which we denote Rabi-like due to the analogy with the field of nuclear magnetic resonances. In this work, we propose a method to achieve a better resolution than the Rabi-like protocol, which consists of two oscillating fields separated in time, which we call Ramsey-like. We focus on BECs in harmonic traps, considering mainly the quadrupole and breathing modes for different trap anisotropy values and comparing the results using single and double excitation zones. First, we employ a variational approach with a Thomas-Fermi ansatz, which gives rise to dynamical equations that are numerically solved. Then, we modeled the problem as a three-level system, offering a concise and alternative description of the same dynamics, enabling the idea of coherent control of these collective modes. Both approaches show that the Ramsey-like protocol provides a better resolution than the Rabi-like. This offers the possibility of measuring collective mode frequencies with higher precision, which is important in experiments where they are used as indirect measurements of properties that are difficult to probe.

1 INTRODUCTION

A hallmark of Bose-Einstein condensation is the emergence of a superfluid phase [1]. This microscopical coherent phenomenon has interesting implications, such as the appearance of collective oscillations in trapped superfluids [2, 3]. These collective oscillations depend on the properties of the system, such as the trap geometry, atom-atom interactions [4], and the presence of defects [5]. Improving the resolution of measurements of collective mode frequencies is essential to enhancing and designing applications where they can be employed as sensors.

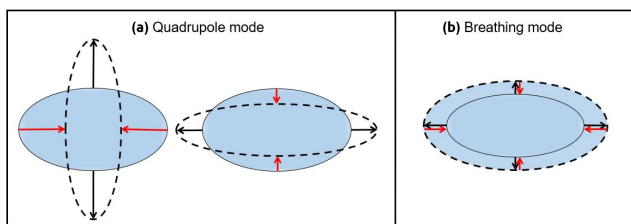


Figure 1: Illustrative representation of (a) the quadrupole mode, exhibiting an out-of-phase oscillation with one axis expanding (black arrow) and the other contracting (red arrow), and (b) breathing mode, where both axes of the BEC can either expand (black arrow) or contract (red arrow) in phase.

Considering harmonically-trapped Bose-Einstein condensates (BECs), among all the collective modes, the quadrupole and breathing modes are both direct consequences of the superfluid property of the system. The quadrupole and breathing modes are characterized by out-of-phase and in-phase radii oscillations, respectively, as illustrated in Figure 1.

The main challenge in designing excitation protocols for these collective modes is to produce perturbations that excite predominantly the desired mode while the other modes are suppressed. Commonly used approaches involve time-periodic modulations of the trapping potential [3, 6–8] and *s*-wave scattering length modulations using Feshbach resonances [4, 9]. Another approach to excite collective modes involves applying an oscillating magnetic field gradient that overlaps with the trap field [10]. So far, this technique has typically followed a standard procedure of keeping the oscillating magnetic field on for a set excitation time. However, it can also be implemented using separate excitation zones, where the field is applied for a specific period, paused, and then reapplied for the same duration.

The excitation protocol previously described is motivated from the Rabi [11] and Ramsey techniques [12, 13] applied in the context of nuclear magnetic resonance to manipulate quantum states through external oscillating fields. The Rabi technique consists in applying an external field to promote spin transitions, whether they are electron or nuclear spins. If the driving frequency matches the frequency associated to the energy difference between two quantum states, the population oscillates sinusoidally between them, phenomenon known as Rabi oscillations [14]. Therefore, the Rabi technique provides a straightforward way to determine resonance frequencies and control populations between states, but has limitations in terms of precision. On the other hand, the Ramsey technique, also known as Ramsey's method of separated oscillatory fields, improves upon the Rabi method by using two zones separated by a free evolution period rather than a continuous oscillating field. The presence of a free evolution period allows the system to acquire a relative phase between the two superposition states, resulting in interference fringes after the second excitation zone. These inter-

ference fringes, known as Ramsey fringes, narrow the resonance peak, thereby enhancing the precision of frequency measurements compared to the Rabi technique. Moreover, the shorter interaction time with the oscillating field minimizes relaxation and dephasing effects, leading to more accurate and stable measurements, which is crucial in quantum coherence experiments. Therefore, leveraging the inherent advantage of the Ramsey protocol over the Rabi method, we have implemented an analogous approach in our Rabi system to probe collective modes in a BEC.

In this work, we considered an oscillating magnetic field gradient that overlaps with the trap field to produce controlled excitations of the collective modes. Moreover, we employ the concept of excitation zones, comparing the results obtained using one and two zones. The latter was conceived in analogy with the separated oscillating fields method, commonly referred to as the Ramsey method [13, 15], vastly used in high-resolution spectroscopy of atoms [16] and interferometry [17], but now using a many-body state as the target.

This work is organized as follows. In Sec. 2, we briefly introduce the collective modes of interest, namely the breathing and quadrupolar modes. Section 3 contains the details of the Rabi and Ramsey-like excitation protocols. In Sec. 4, we introduce a variational approach and the numerical solutions to the resulting differential equations. Section 5 deals with the three-level model and its dynamics, which is employed under the light of coherent population control in Sec. 6. Finally, we present our conclusions in Sec. 7.

2 COLLECTIVE MODES

In the mean-field approach, the dynamics of a weakly interacting condensate can be described by the time-dependent Gross-Pitaevskii equation (GPE),

$$i\hbar \frac{\partial \psi}{\partial t} = \left(-\frac{\hbar^2}{2m} \nabla^2 + V(\mathbf{r}, t) + g|\psi(\mathbf{r}, t)|^2 \right) \psi, \quad (1)$$

where $g = 4\pi\hbar^2 a_s/m$ with m being the atomic mass and a_s the s -wave scattering length. In this work, we considered an axially symmetric harmonic oscillator trapping potential given by

$$V_{\text{trap}}(r) = \frac{m\omega_r^2}{2}(x^2 + y^2 + \lambda^2 z^2), \quad (2)$$

where $\lambda = \omega_z/\omega_r$ is the anisotropy factor responsible for the shape of the BEC.

Considering the regime of small deviations around the equilibrium density, where the system preserves its coherence, we can assume a linear regime and use the hydrodynamical formalism [18] to obtain the frequencies of the collective modes. Among all the possible solutions given in terms of spherical harmonics $Y_{\ell m}(\theta, \phi)$, we focus on the coupled breathing ($\ell = 0, m = 0$) and quadrupole ($\ell = 2, m = 0$) modes. In this regime, the frequency of these low-lying modes is given by [18]

$$\omega_{Q,B} = \omega_r \left(2 + \frac{3}{2}\lambda^2 \pm \frac{1}{2}\sqrt{16 - 16\lambda^2 + 9\lambda^4} \right)^{1/2}, \quad (3)$$

where the plus sign is related to the frequency of the breathing mode ω_B while the minus sign denotes the frequency of the quadrupolar mode ω_Q .

3 EXCITATION PROTOCOL

The potential term $V(\mathbf{r}, t)$ in Eq. (1) is the sum of the trapping potential, Eq. (2), and an external potential responsible for exciting the quadrupole and the breathing modes. We considered a perturbative potential given by

$$V_{\text{osc}}(z, t) = \lambda^2 A f(t) \xi(t) z^2, \quad (4)$$

where $\xi(t)$ represents a modulating signal, and the oscillating function is chosen to be

$$f(t) = 1 - \cos(\omega_{\text{exc}} t), \quad (5)$$

introducing the driving frequency ω_{exc} . The constant A determines the perturbation strength and has units of energy per length squared. Excitation potentials such as this one can be created through magnetic field gradients, and this particular form is inspired by the experimental setup in Refs. [19–21].

Considering the contribution of both the trapping and excitation potentials, we have

$$V(r, z, t) = \frac{m\omega_r^2}{2} \left[r^2 + \lambda^2 \left(1 + \frac{2A f(t) \xi(t)}{m\omega_r^2} \right) z^2 \right], \quad (6)$$

where $r^2 = x^2 + y^2$. This potential describes a time-dependent modulation along the z -direction corresponding to either an expansion or a squeezing along this direction, depending on the value of the term inside the parenthesis.

One of the simplest choices for the modulating signal is a single rectangular pulse,

$$\xi(t) = \begin{cases} 1, & 0 \leq t \leq t_{\text{exc}}, \\ 0, & \text{otherwise,} \end{cases} \quad (7)$$

where t_{exc} is the duration of the excitation, as illustrated in Figure 2. We denote this as the Rabi-like signal, in analogy with the work of Rabi in the field of spin magnetic resonance [11].

Following the same analogy, we can define a Ramsey signal, drawing a parallel with what Ramsey did to enhance the resolution of the Rabi technique [12]. The Ramsey signal can be written as

$$\xi(t) = \begin{cases} 1, & 0 \leq t \leq t_{\text{exc}}, \\ 0, & t_{\text{exc}} < t \leq t_{\text{exc}} + t_{\text{free}}, \\ 1, & t_{\text{exc}} + t_{\text{free}} < t \leq 2t_{\text{exc}} + t_{\text{free}}, \\ 0, & \text{otherwise,} \end{cases} \quad (8)$$

where t_{free} is the interval between the two perturbative pulses when the system evolves freely. The Ramsey protocol involves the separation of the Rabi pulse into two distinct excitation zones, as illustrated in Figure 2. The key concept behind this procedure is that the time interval t_{free} between the excitation zones introduces a phase difference in the system, which might give rise to interference phenomena.

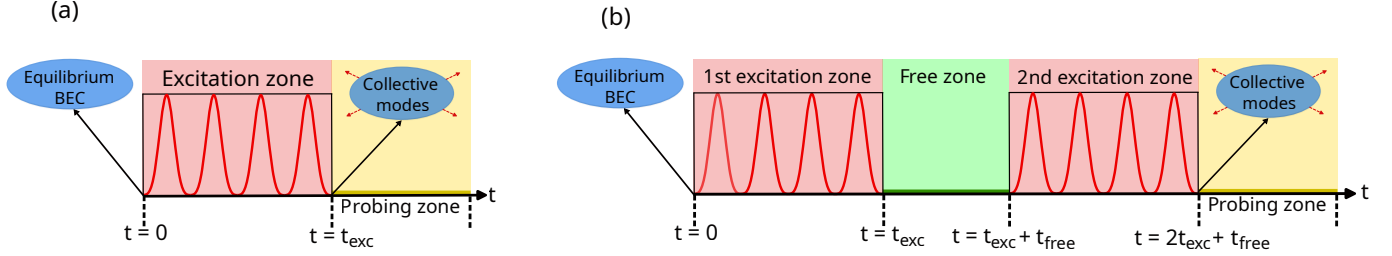


Figure 2: (a) Temporal diagram illustrating the Rabi protocol to excite a BEC. We start with an equilibrium BEC at $t = 0$. Subsequently, a single pulse with a duration of t_{exc} is applied. The probing zone refers to times where the excitation protocol ceased, allowing observation of the BEC. (b) Temporal diagram illustrating the Ramsey protocol to excite a BEC. Unlike the Rabi protocol, just after the first excitation zone the system evolves freely during a time t_{free} until the second excitation zone, also with duration t_{exc} , starts at $t = t_{\text{free}} + t_{\text{exc}}$.

4 VARIATIONAL METHOD

4.1 Thomas-Fermi ansatz

We start by considering a trial wave function based on the Thomas-Fermi profile [4, 18],

$$\begin{aligned} \psi(\mathbf{r}, t) = & \sqrt{n_0 \left(1 - \frac{x^2}{R_x^2} - \frac{y^2}{R_y^2} - \frac{(z-z_0)^2}{R_z^2} \right)} \\ & \times e^{i[\alpha_1 x + \alpha_2 y + \alpha_3 (z-z_0)]} e^{i[\beta_1 x^2 + \beta_2 y^2 + \beta_3 (z-z_0)^2]} \\ & \times \Theta \left(1 - \frac{x^2}{R_x^2} - \frac{y^2}{R_y^2} - \frac{(z-z_0)^2}{R_z^2} \right), \end{aligned} \quad (9)$$

where R_i are the Thomas-Fermi radii, Θ is the Heaviside step function, the peak density is given by $n_0 = 15N/(8\pi R_x R_y R_z)$, and we have introduced 9 time-dependent variational parameters: $\{R_i, \alpha_i, \beta_i\}$. The phase term in Eq. (9) is essential because it provides the necessary degrees of freedom for the oscillations to take place [22].

Using the trial wave function of Eq. (9), we applied the variational method [23, 24] to obtain the dynamical equations for the BEC radii along each direction,

$$\frac{\partial^2 \bar{R}_x}{\partial \tau^2} + \bar{R}_x = \frac{P_0}{\bar{R}_x \bar{R}_y \bar{R}_z}, \quad (10)$$

$$\frac{\partial^2 \bar{R}_y}{\partial \tau^2} + \bar{R}_y = \frac{P_0}{\bar{R}_x \bar{R}_y \bar{R}_z}, \quad (11)$$

$$\frac{\partial^2 \bar{R}_z}{\partial \tau^2} + \lambda^2 \bar{R}_z = \frac{P_0}{\bar{R}_x \bar{R}_y \bar{R}_z} - \lambda^2 \bar{A} f(\tau) \xi(\tau) \bar{R}_z, \quad (12)$$

written in a dimensionless form. This is achieved by expressing lengths in terms of the harmonic oscillator length $\ell_0 = (\hbar/m\omega_r)^{1/2}$, energies in units of $\hbar\omega_r$, and time in ω_r^{-1} , leading to $\bar{R}_i = R_i/\ell_0$, $\tau = t\omega_r$, $\bar{A} = A\ell_0^2/\hbar\omega_r$, and $P_0 = 15Na_s/\ell_0$. These equations are consistent with Ref. [25].

4.2 Fixed excitation frequency

This approach gives us Newton-like equations, Eqs. (10)–(12), governing the BEC radii with straightforward interpretation.

The left-hand side of the equations corresponds to the harmonic oscillator components. The terms proportional to P_0 are due to the interatomic interactions, which can either localize or expand the cloud, depending on whether they are attractive or repulsive. The term proportional to \bar{A} , only present in the dynamical equation for the z -direction, denotes the role of the external excitation. By construction, the variational method is robust enough to capture additional types of dynamics besides the collective modes as long as the BEC shape resembles the assumed Thomas-Fermi profile.

We numerically solved Eqs. (10)–(12) by employing a fourth-order Runge-Kutta method. Our starting point is a ^{87}Rb BEC with $N = 10^5$ atoms, a s -wave scattering length of $a_s = 100a_0$, and a radial frequency of the trap $\omega_r = 2\pi \times 200$ Hz. We obtained the initial conditions by solving the Eqs. (10)–(12) neglecting the time derivatives. Since our system holds cylindrical symmetry, the time evolution of both \bar{R}_x and \bar{R}_y will be the same. Thus, as from now, they will be referred as the radial radius \bar{R}_r .

To produce the radii oscillations, we set the driving frequency $\bar{\omega}_{\text{exc}} = 1$, the excitation amplitude $\bar{A} = 0.05$, and the excitation and free times $\tau_{\text{exc}} = \tau_{\text{free}} = 32$. In Table 1, it is possible to see the corresponding quadrupole and breathing frequencies obtained using Eq. (3) considering different values of λ .

To measure the frequencies of the collective modes, we investigate the evolution of the BEC radii after the perturbation has ceased for a fixed excitation frequency $\bar{\omega}_{\text{exc}} = 1$. Figure 3 shows the Fourier Transform (FT) of the time evolution of the BEC radii after the excitation protocol using both Rabi and Ramsey signals. The peaks depend on the modulation of the external signal, indicating different coupling to the collective modes. Although some cases display multiple peaks, the ones with higher amplitudes are at the expected frequencies for the quadrupole and breathing modes.

Figure 3 shows that the perturbation excites the quadrupole mode more than the breathing mode for $\lambda \leq 1$. In the case of $\lambda = 1/9$ [Figs. 3(a), (e), (i), (m), and (q)], the breathing mode is barely excited. As we decrease the anisotropy of the trap, the amplitude of the breathing mode becomes appreciable, although the quadrupole mode is still more relevant for $\lambda \leq 1$. This can be attributed to two main factors: the excitation was applied along the z -direction, favoring an out-of-phase oscillation; the quadrupole mode is more easily excited due to the lower confine-

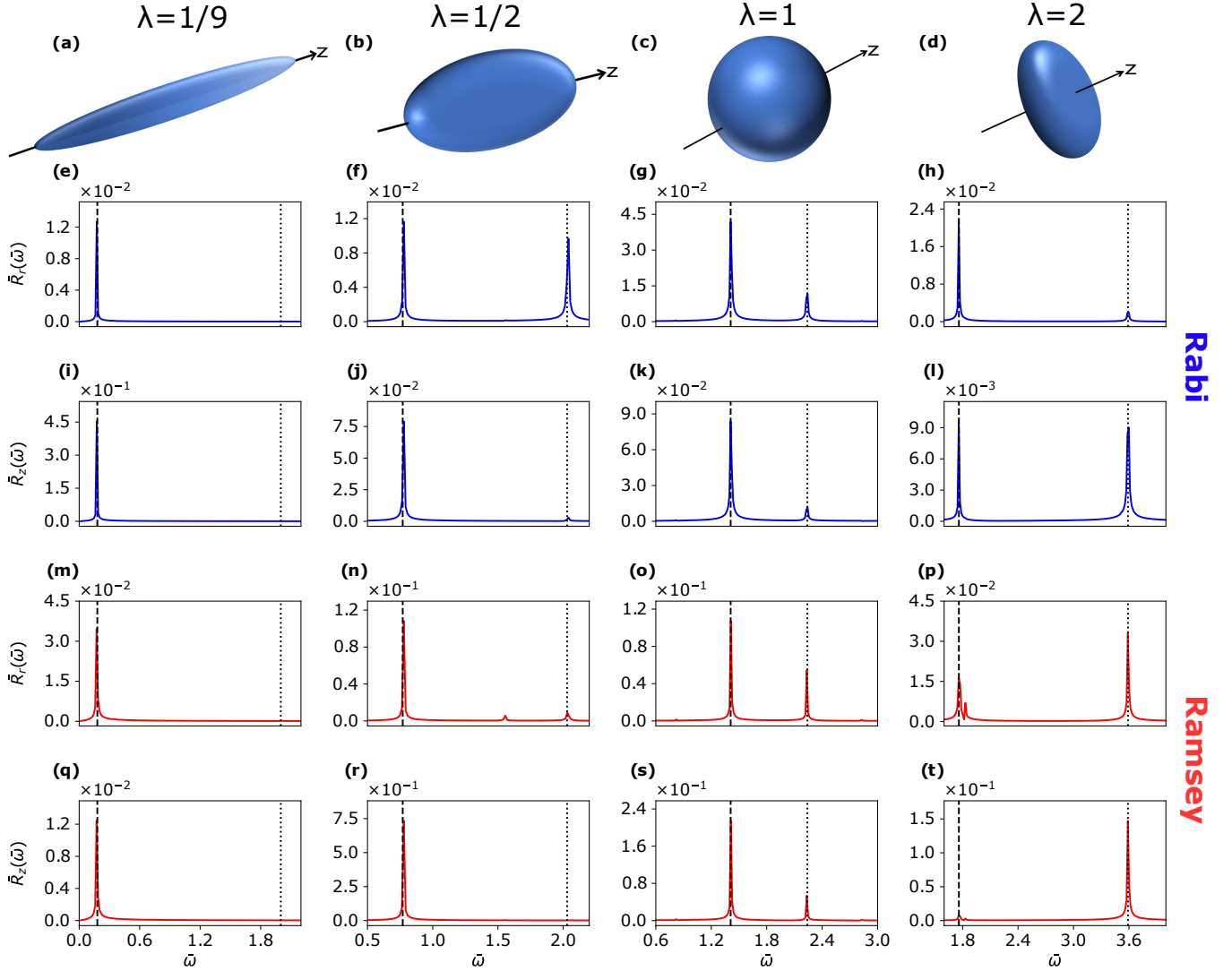


Figure 3: Fourier transforms of the radii oscillations of the BEC. Two different protocols were used to excite the collective modes: the Rabi-like is denoted by blue curves, while red curves indicate the Ramsey-like protocol. We employed the excitation parameters: $\bar{A} = 0.05$, $\bar{\omega}_{\text{exc}} = 1$, $\tau_{\text{exc}} = 32$, and $\tau_{\text{free}} = 32$. Each column corresponds to a different trap anisotropy, $\lambda = 1/9, 1/2, 1$, and 2 . The dashed and dotted lines correspond to the expected frequency for the quadrupole and breathing modes according to Eq. (3), respectively.

ment in the z -direction. An interesting scenario is when there is an inversion of the confining strength. For $\lambda = 2$ [Figs. 3(d), (h), (l), (p), and (t)], the radial direction becomes more confining than the z -direction, and the amplitude of the breathing mode can be of the order of the quadrupole mode and even larger in some cases.

There are peaks at positions other than the quadrupole and breathing frequencies. Some of them correspond to $\bar{\omega}' = \bar{\omega}_B - \bar{\omega}_Q$, i.e., an intermediate state between the breathing and quadrupole modes transition. For $\lambda = 2$, where $\bar{\omega}' = 1.83$ is close to the quadrupole frequency (generating beating effects in the radii oscillations), it can be seen in Figure 3(p) and (t). In the case of $\lambda = 1$, the peak located at the frequency $\bar{\omega}' = 0.82$ has a much smaller magnitude. In Figure 4, we zoom in on the region

of the peaks for better visualization and we compared the Rabi and Ramsey protocol. This example illustrates the advantage of the Ramsey-like protocol over the Rabi-like since these peaks appear more clearly using the Ramsey protocol, indicating that this signal offers enhanced frequency resolution. The additional peak present in graph (n) of Figure 3 is located at the frequency $\bar{\omega} = 1.54$, which is twice the frequency of the quadrupole mode for $\lambda = 1/2$. Its manifestation occurs due to the non-linear contribution of the hydrodynamical equations [26, 27], a process similar to what happens in non-linear optics when there is the second harmonic generation [28].

4.3 Resonance curves

As previously discussed, the Ramsey method offers a significant advantage over the Rabi method in achieving higher precision

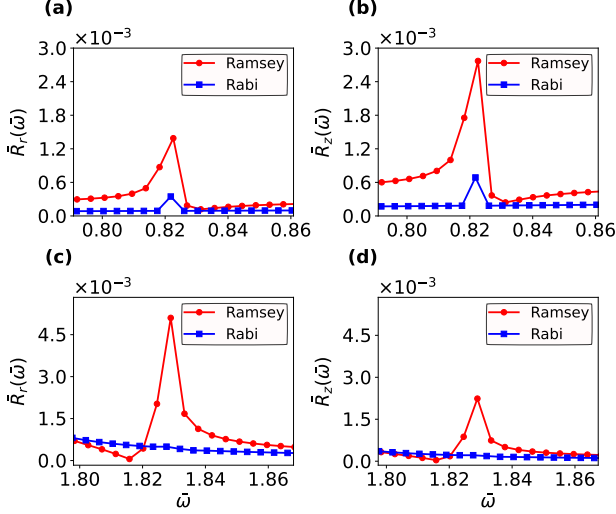


Figure 4: Fourier spectrum of the radii oscillation of the BEC using the Rabi and the Ramsey protocols for both $\lambda = 1$ and $\lambda = 2$, evidencing the contribution of a mode to the radii oscillations with frequency given by the difference between the frequency of the breathing and quadrupole mode ($\bar{\omega}' = \bar{\omega}_B - \bar{\omega}_Q$). While graphs (a) and (b) plot the Fourier spectrum of the radial and z -directions, respectively, considering $\lambda = 1$, graphs (c) and (d) present the same plot but for $\lambda = 2$.

in measuring system resonances. In this section, we aim to construct the resonance curves of the collective modes using both the Rabi and Ramsey excitation protocols, subsequently comparing the accuracy provided by each approach.

To construct the resonance curves, we have to repeat the procedure of Figure 3, which was obtained with $\bar{\omega}_{\text{exc}} = 1$, for other values of the excitation frequency. Then, we select the maximum amplitude observed in the FT for a given mode (quadrupole or breathing), radius (R_r or R_z), anisotropy factor, signal, and excitation frequency. This becomes one point in the resonance curve; the others are obtained by varying the excitation frequency. We adopted the same excitation parameters as in the case of Figure 3, i.e., we set $\bar{A} = 0.05$ and $\tau_{\text{exc}} = \tau_{\text{free}} = 32$, while we varied the excitation frequency $\bar{\omega}_{\text{exc}}$ in the range from 0.1 to 4.2. These parameters were chosen to obtain a clear interference pattern in the resonance curve, to be compatible with typical experiments [19, 21, 29], and to keep the system in the so-called coherent regime, i.e., where the modes which are excited are mainly the desired collective modes. Yet, the most effective way to attain a well-defined resonance curve is to extend as much as possible the excitation time in such a way that each external frequency will undergo a greater number of oscillation cycles, resulting in a clearer and more distinct resonance curve. Nevertheless, aiming to simulate experimental conditions, we kept the excitation parameters as previously described.

Figure 5 summarizes our findings. The most notable feature is the appearance of Ramsey fringes when the protocol with the two excitation zones is applied, in analogy with Ramsey's interferometry method [13]. The consequence is that, both in interferometry and in our case, the Ramsey method yields

narrower peaks than the Rabi protocol, providing better accuracy in frequency measurements.

For a two-level quantum system subject to a sinusoidal-like external perturbation, the solution for the transition probability is well-known and straightforward obtained for both Rabi and Ramsey case [14]. The Rabi case provides an exact solution whose functional form is given by

$$R(\Delta) = A \left(\frac{\sigma^2}{\Delta^2 + \sigma^2} \right) \sin^2 \left(B \sqrt{\sigma^2 + \Delta^2} \right), \quad (13)$$

which is a Lorentzian function being modulated by the $\sin^2(b \sqrt{\sigma^2 + \Delta^2})$ function, where A, B and σ are parameters to be adjusted and $\Delta = \bar{\omega}_{\text{exc}} - \bar{\omega}_{Q,B}$ is the detuning. Aiming to estimate the error as the full width at half maximum (FWHM) of the graph, we are led to a transcendental equation

$$\sin \left(B \sqrt{\sigma^2 + \Delta^2} \right) = \frac{\Delta}{\sqrt{2AB\sigma}}, \quad (14)$$

where its solution in the frequency range delimited by the main peak allows us to compute the width. Likewise, the Ramsey functional form is given by

$$R(\Delta) = A \text{sinc}^2(B\Delta) \cos^2(C\Delta), \quad (15)$$

which is a Rabi envelope being modulated by a $\cos^2(C\Delta)$ function and, once again, A, B and C are parameters to be adjusted. The $\cos^2(C\Delta)$ term is responsible for generating the interference fringes, thus, the amplitude falls to its half when $C\Delta = \pi/4$. Thereby, the width for the Ramsey resonance curve can be obtained through

$$\delta\bar{\omega} = \frac{\pi}{2C}. \quad (16)$$

Indeed, the ideal Ramsey experiment predicts $\delta\bar{\omega} = \pi/t_{\text{free}}$, which for our parameters results in $\delta\bar{\omega} = 0.098$.

To fit our data on both functions (13) and (15), we used, for convenience, the radial direction since all values of λ show a resonance curve when computed along this direction. Table 1 displays the results of the calculated resonance frequency for each collective mode considering the uncertainty associated to both Rabi and Ramsey resonance curves. As expected, for all cases, the Ramsey protocol has proven to be the method which provides the closest value from the expected result according to Eq. (3).

The $\lambda = 1/2$ case [Figs. 5(b), (f), (j), and (n)] is illustrative of differences between the two excitation protocols. In fact, looking at the central peak of the interference pattern for $\lambda = 1/2$, there is a slight shift between the central peak of Rabi and Ramsey curves.

Although the resonance curves present a much more precise alternative for determining the frequencies of the collective modes, they cannot resolve modes that are absent in the FT spectrum. This is the case of the breathing mode in the z -direction for $\lambda = 1/9$, which is barely manifested in the FT spectrum [Figure 4(e), (l), (m), (q)]. The same happens in the resonance curve, where there is no interference pattern, Figure 5(m). Also, when we take the quadrupole mode into account, the resonance pattern is not well-defined. This is primarily because the quadrupole frequency is relatively small, and the chosen excitation time is insufficient to complete even a single period of excitation.

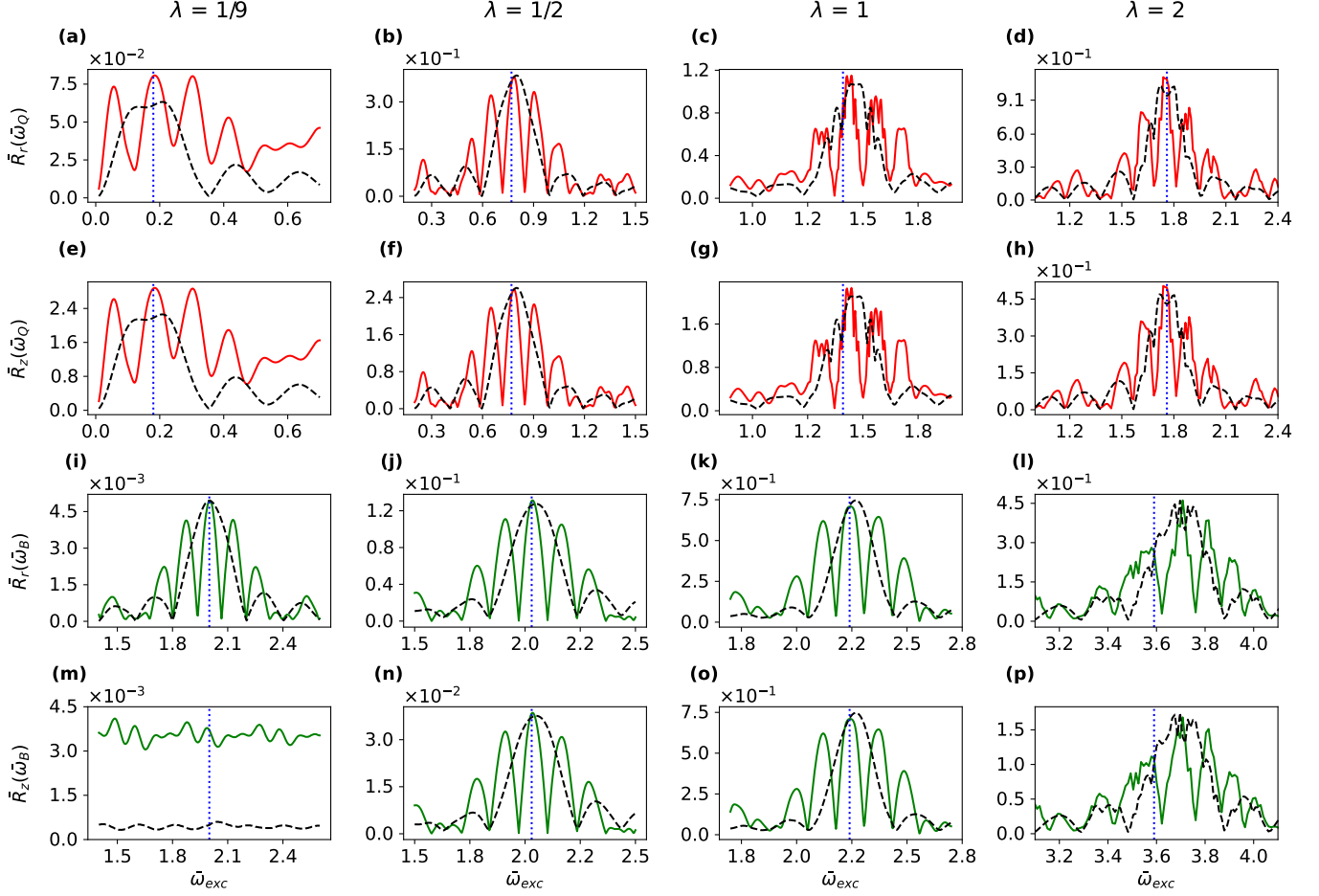


Figure 5: Resonance curves for both quadrupole (red line) and breathing (green line) modes for $\lambda = 1/9$, $\lambda = 1/2$, $\lambda = 1$ and $\lambda = 2$ considering both Rabi (dashed line) and Ramsey (solid line) excitation protocols. The used excitation parameters were $\bar{A} = 0.05$, $\tau_{\text{exc}} = 32$ and $\tau_{\text{free}} = 32$. The vertical dotted line denotes the expect resonance frequency according to Eq. (3). Each column corresponds to a different trap anisotropy, $\lambda = 1/9, 1/2, 1$, and 2 .

Table 1: Quadrupole and breathing mode frequencies calculated using Eq. (3), the Rabi fitting (Eq. (13)), and the Ramsey fitting (Eq. (15)), considering the variational method and the three-level model for four different values of anisotropy λ . On the left side of this table, we summarize the resonance frequencies and their associated uncertainties obtained for the quadrupole mode, while on the right side, we provide the same information for the breathing mode.

λ	Variational					Three-level				
	Eq. (3)	Rabi	Ramsey	Rabi	Ramsey	Eq. (3)	Rabi	Ramsey	Rabi	Ramsey
$\lambda = 1/9$	$\bar{\omega}_Q$	$\bar{\omega}_Q$	$\bar{\omega}_Q$	$\bar{\omega}_Q$	$\bar{\omega}_Q$	$\bar{\omega}_B$	$\bar{\omega}_B$	$\bar{\omega}_B$	$\bar{\omega}_B$	$\bar{\omega}_B$
1/9	0.18	0.2(2)	0.18(6)	0.2(2)	0.18(6)	2.00	2.0(2)	2.00(7)	2.0(2)	2.00(6)
1/2	0.77	0.8(2)	0.77(7)	0.8(1)	0.77(6)	2.03	2.1(2)	2.03(7)	2.0(1)	2.03(7)
1	1.41	1.5(2)	1.45(6)	1.4(1)	1.41(4)	2.24	2.3(2)	2.24(6)	2.2(2)	2.24(6)
2	1.76	1.7(2)	1.74(6)	1.7(2)	—	3.59	3.7(2)	3.71(8)	3.6(5)	—

Given that the perturbative term in the dynamical equation 12 along the z -direction scales with λ^2 , for $\lambda \geq 1$, the perturbation strength is notably amplified. In this scenario, the system starts to deviate from the coherent regime as seen in Figs. 5(c), (g), (d), (h), (l), and (p). Once excitations are amplified, higher energy modes contribute to a non-coherent behavior leading to a large phase fluctuation of the wave function. In the cases where other excitations play a major role in the system, as observed mainly in the resonance curves of the quadrupole mode for $\lambda = 1$ (Figs. 5(c) and (g)) and breathing mode for $\lambda = 2$ (Figs. 5(l) and (p)), there is an evident shift between the frequency predicted by Eq. (3) and the one calculated thorough the Rabi (Eq. (13)) and Ramsey (Eq. (15)) fitting, as shown in Table 1. It turns out that since the manifestation of collective modes depends on the interactions in the system, other types of fluctuations, whether they are quantum or thermal, act as an effective interaction, leading to a shift in the collective modes frequencies [30–32].

Although we do not have any dissipation in the system, such as the presence of a thermal cloud, the superfluid component itself might contribute to transfer of modes in the collective oscillations. As the external perturbations are introduced on a similar spatial scale as the system, the low-lying collective modes with wavelengths of the order of the BEC radii represent the first excited modes. However, the energy contained in these modes is transferred to modes with higher momentum k , described by the Bogoliubov spectrum [33]. This transfer occurs due to the non-linearity of the GPE, facilitating the energy transfer to higher-lying modes through mode mixing, which results in a dissipation of the population of the collective modes. Indeed, to obtain the frequencies of the collective modes, we used a linear approximation in the hydrodynamic equations, which is no longer a good approximation for high excitation amplitudes. This dissipation and the presence of other modes besides the collective ones introduce non-coherent effects, which make the system deviate from the scenario of complete coherence.

5 THREE-LEVEL MODEL

Motivated by the results obtained from the numerical solutions of the dynamical equations and the fact that we are considering a regime where the system preserves a high degree of coherence, we propose an alternative description of the dynamics of the collective modes. The resonance curves exhibit narrow widths, supporting the idea of single quantum states rather than considering a band. In this sense, this can be modeled as a three-level quantum system, as illustrated in Figure 6, in analogy with a three-level atom subject to an external perturbation. The lowest level, labeled as $|1\rangle$, corresponds to the ground-state BEC, the middle to the quadrupole mode ($|2\rangle$), and the upper level to the breathing mode ($|3\rangle$).

Using the canonical quantization and working in the interaction picture, the perturbative potential in Eq. (4) is considered now an operator written as

$$\hat{V}_{\text{osc}}(t) = f(t) \sum_{i,j} \hbar \Omega_{ij} e^{-i(\omega_j - \omega_i)t} |i\rangle \langle j|, \quad (17)$$

where we defined Rabi-like frequencies as

$$\Omega_{ij}(A, \lambda) = \frac{\lambda^2 A}{\hbar} \langle i | \hat{z}^2 | j \rangle. \quad (18)$$

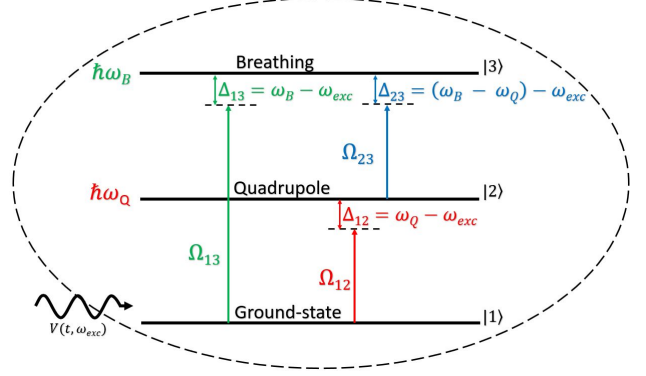


Figure 6: Three-level system under an external perturbation. The upper level is related to the breathing mode, the intermediate level is related to the quadrupole mode, and the lower level stands for the BEC at rest.

Hence, to have access to the Rabi-like frequencies of this system we have to compute the matrix elements of the operator \hat{z}^2 . The diagonal matrix elements of this operator are non-zero, in contrast with dipole-like operators [34]. Despite this, these elements remain inactive in the dynamics as they do not contribute to the coupling between the modes. They only contribute as a global phase, which does not change the quantum state.

The inner product $\langle i | \hat{z}^2 | j \rangle$ carries significant meaning regarding the coupling of collective modes in the system. Its value indicates which transitions are more likely to occur. Since changes in the geometry of the confining potential alter the coupling of these modes, it is reasonable to expect that this inner product will depend on λ . Consequently, Eq. (18) will exhibit a dependence on λ different from that λ^2 initially suggested.

This whole scenario gives rise to three possible transitions $|1\rangle \rightarrow |2\rangle$, $|1\rangle \rightarrow |3\rangle$, and $|2\rangle \rightarrow |3\rangle$, where two of them contribute to the population of the breathing mode. Consequently, one can reasonably anticipate the emergence of two main peaks in the resonance curve of the breathing mode: one positioned at ω_B and another at $\omega' = \omega_B - \omega_Q$. Each of the three transitions has its own Rabi frequency, reflecting the coupling strength with the external excitation, where higher values of Rabi frequency suggest preferential population transfer to the associated state.

A convenient way to describe the dynamics of the system is through the density operator formalism. The dynamics of this quantum closed system can be computed by evolving the density operator $\hat{\rho}(t) \equiv |\Psi(t)\rangle \langle \Psi(t)|$ with the master equation [35, 36]

$$\frac{d\hat{\rho}(t)}{dt} = \frac{i}{\hbar} [\hat{\rho}(t), \hat{V}_{\text{osc}}(t)]. \quad (19)$$

Since the potential $\hat{V}_{\text{osc}}(t)$ in Eq. (17) commutes at different times, i.e., $[\hat{V}_{\text{osc}}(t), \hat{V}_{\text{osc}}(t')] = 0$, the general solution of Eq. (19) is given by

$$\hat{\rho}(t) = \hat{U}(t, t_0) \hat{\rho}(t_0) \hat{U}^\dagger(t, t_0), \quad (20)$$

where

$$\hat{U}(t, t_0) = \exp\left(-\frac{i}{\hbar} \int_{t_0}^t \hat{V}_{\text{osc}}(t') dt'\right) \quad (21)$$

is the time evolution operator in the interaction picture.

To numerically solve this equation, we followed the time discretization described in Ref. [37, 38] using the Strang splitting scheme. Since we initially have a BEC in equilibrium, we considered that all population starts in the ground state at $t = 0$. Then, we use Eq. (19) to obtain the evolution of the population (or transition probability) of each state, as well as the coherence between them over time. We can construct resonance curves, as we did with the variational method. The main distinction is that instead of employing the BEC radii, we use the populations of the three modes. This simple model presents a versatile framework, provided that we compute the Rabi-like frequencies associated with the distinct applied excitations. Unlike atomic systems, this model has no decay mechanisms, although their inclusion could lead to a better description in cases with larger excitation amplitudes.

In principle, computing the Rabi-like frequencies can be achieved through two approaches. Firstly, by evaluating the inner product,

$$\langle i | \hat{z}^2 | j \rangle = \int_{-\infty}^{+\infty} \psi_i^* z^2 \psi_j d^3 \mathbf{r} = g(\lambda), \quad (22)$$

where ψ_i and ψ_j are the wave functions representing each coherent state in the model. However, defining who are the wave function explicitly is not a simple task.

The second method is to scan a wide interval of Rabi-like frequencies and finding the values which better reproduce the interference pattern of the variational results for a giving coupling strength. This will be the method adopted in this work. In this sense, our goal was to minimize the Mean Squared Error (MSE) or chi-squared [39] defined by

$$\chi^2 = \frac{1}{\bar{\omega}_{exc}^{max} - \bar{\omega}_{exc}^{min}} \int_{\bar{\omega}_{exc}^{min}}^{\bar{\omega}_{exc}^{max}} (\bar{U}(\bar{\omega}_{exc}) - \bar{\rho}_{ii}(\bar{\omega}_{exc}))^2 d\bar{\omega}_{exc}, \quad (23)$$

where $\bar{U} = \bar{R}_r / \max(\bar{R}_r)$ and $\bar{\rho}_{ii} = \rho_{ii} / \max(\rho_{ii})$. The result of this minimization through Eq. (23) can be seen in Figure 7, where we compare the resonance curves obtained with both the three-level model and the variational method, adopting the same excitation parameters in both cases ($\bar{A} = 0.05$, $\tau_{exc} = \tau_{free} = 32$). The resulted Rabi-like frequencies can be seen in Table 2 plotted in Figure 9.

Table 2: Rabi frequencies of the three transitions contributing to the population of the quadrupole ($\bar{\Omega}_{12}$) and breathing ($\bar{\Omega}_{13}$ and $\bar{\Omega}_{23}$) modes obtained from the three-level model for four different values of the anisotropy factor λ .

λ	$\bar{\Omega}_{12}$	$\bar{\Omega}_{13}$	$\bar{\Omega}_{23}$
1/9	0.0149(1)	0.004(1)	0.002(1)
1/2	0.11(1)	0.009(1)	0.0052(2)
1	0.08(2)	0.13(2)	0.09(1)
2	0.04(1)	0.260(1)	0.177(1)

Notably, the three-level model can qualitatively reproduce the same patterns we obtained using the variational model. For $\lambda = 1/9$, all the Rabi frequencies exhibit relatively low values, confirming that the system is barely excited, as expected from the

variational results. Yet, the system presents a higher excitation of the quadrupole mode.

The Rabi quadrupole transition frequency $\bar{\Omega}_{12}$ is significantly larger than the other frequencies for values of $\lambda < 1$, which agrees with the results obtained using the variational approach, where the quadrupole mode is predominantly excited. However, this behavior changes when $\lambda \geq 1$. For $\lambda = 1$, all the Rabi-like frequencies have similar magnitudes and thus, the breathing and the quadrupole modes are equally likely to be populated. Indeed, this is aligned with the result obtained through the variational method, where the breathing mode began to have a significant role in the system, unlike the case for $\lambda = 1/9$ and $\lambda = 1/2$. Notably, $\bar{\Omega}_{12}$ is larger than the one for $\lambda = 1/9$ and similar to the one for $\lambda = 1/2$. This indicates that the excitation of the quadrupole mode for $\lambda = 1$ and $1/2$ will be similar, but greater than that in the case of $\lambda = 1/9$, also in agreement with the resonance curves of the variational method along the radial direction.

We should point out some important differences between the variational and three-level models, which are even more evident for values of $\lambda \geq 1$. While the three-level model depicts a coherent system by construction, the variational model captures additional types of fluctuations as long as they adhere to the Thomas-Fermi profile, Eq. (9). Consequently, the variational approach provides other forms of fluctuations beyond collective modes, such as elementary excitations of the Bogoliubov spectrum which may contribute as a broadening effect in the resonance curve. In contrast, the three-level model does not account for these features. Therefore, it is reasonable to anticipate that for high energy inputs, other non-coherent fluctuations will play a significant role in the system. This behavior is seen in Figs. 7(c) and (f) for both Rabi and Ramsey excitations with $\lambda = 1$ and in Figs. 8(a) and (b) for the Rabi excitation with $\lambda = 2$, where the system leaves the coherent regime and the interference pattern is no longer well-defined, mainly for the Ramsey case. However, as the system still maintains a degree of coherence, considering only the the Rabi method for $\lambda = 2$, it was still possible to estimate a set of Rabi frequencies which makes the resonance of the three-level system roughly match the variational one. In this case, the Rabi frequencies are at least ten times larger than those for $\lambda = 1$. Furthermore, the width calculated from the resonance curve using the three-level model, particularly when fluctuations play a significant role [Figs. 7(c) and (f), and 8(a) and (b)], exhibits lower values compared to those obtained via the variational method (Table 1), fact that reinforces that while the variational method accommodates other type of fluctuations, the three-level model remains coherent by construction.

In analogy with an atom being irradiated by a laser beam, the system may undergo the so-called Landau-Zener tunnelling [40, 41] at high Rabi frequencies, in which the energy of the system is exchanged between the available levels through a non-adiabatic process. This may result in a breakdown of the coherent dynamics of the system, possibly explaining what we have observed in this context.

Comparing Figs. 8(a)-(b), an inversion in the magnitude of the quadrupole and breathing modes is evident. In this case, the quadrupole mode is even more excited at the frequency resonant with the breathing mode frequency, as seen in Figure 8(a), in-

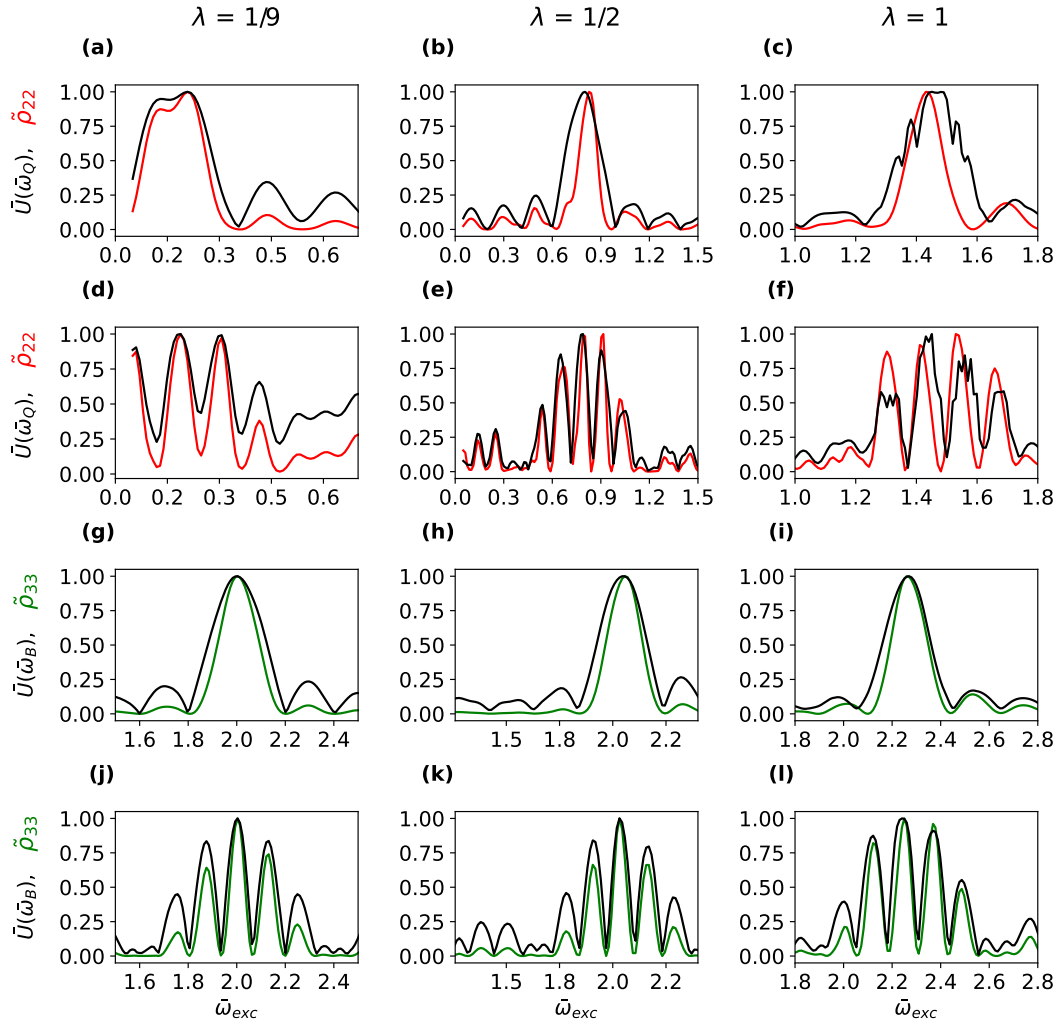


Figure 7: Comparison between the normalized resonance curves of the quadrupole (red line) and breathing (green line) modes obtained from the three-level model and those obtained from the variational method (black line) considering both Rabi [graphs (a)-(c) and (g)-(i)] and Ramsey excitation protocols [graphs (d)-(f) and (j)-(l)]. Each column corresponds to a different trap anisotropy, $\lambda = 1/9, 1/2,$ and 1 .

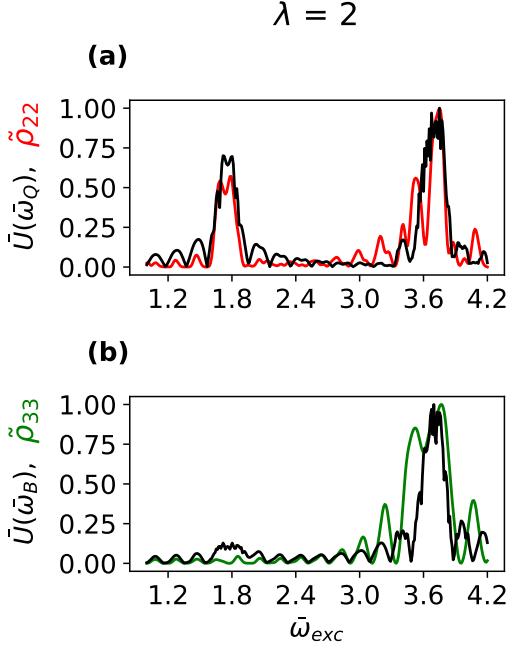


Figure 8: Comparison between the normalized resonance curves of the quadrupole (red line) and breathing (green line) modes obtained from the three-level model and those obtained from the variational method (black line) considering the Rabi excitation protocol for $\lambda = 2$

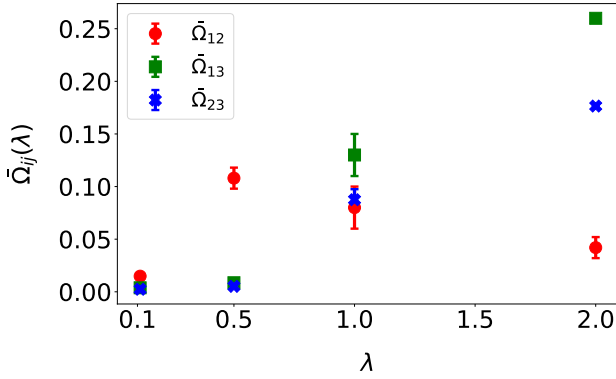


Figure 9: Rabi-like frequencies numerically evaluated respectively to each transition in the three-level model considering four values of the anisotropy factor λ . The excitation parameters used were $\bar{A} = 0.05$ and $\tau_{\text{exc}} = 32$.

dicating its strong coupling to the breathing mode in the oblate geometry. Therefore, we conclude that the Rabi frequency has a strong dependence on λ since changing the trap geometry will significantly impact the coupling between modes.

6 COHERENT POPULATION CONTROL OF COLLECTIVE MODES

The framework provided by the three-level model allows us to approach the dynamics of the collective modes under the light

of coherent control, which has been widely used in spectroscopy experiments [16, 42]. The idea is to use the framework set forth by Rabi and Ramsey to excite and study the collective modes individually.

The three-level model contains three possible transitions. Thus, we can select a specific transition of interest and then tune the external frequency to be resonant with it. Moreover, given our understanding of the Rabi frequencies, we can strategically apply either a π - or $\pi/2$ -pulse to manage the population dynamics of the desired coherent mode as has been done in several interferometry experiments [43–45]. A π -pulse consists in the application of a resonant pulse with a duration of $t_{\text{exc}} = \pi/\Omega_{ij}$ resulting in a complete transfer of population from one quantum state i to another one j . Similarly, a $\pi/2$ -pulse is a resonant pulse with a duration of $t_{\text{exc}} = \pi/2\Omega_{ij}$ that transfers half of the population and places the system into a superposition state. When two $\pi/2$ -pulses are applied sequentially with a time interval in between, the system accumulates a phase difference, which can lead to interference effects.

Figure 10 demonstrates the population control of the quadrupole and breathing modes for $\lambda = 1/2$ using both Rabi and Ramsey excitation protocols. To exclusively excite the quadrupole mode (ρ_{22}), we employed the Rabi protocol (Figure 10(a)), where the external frequency was set resonant with the quadrupole frequency. The excitation was applied with an amplitude $\bar{A} = 0.05$ over a duration $\tau_{\text{exc}} = \pi/\tilde{\Omega}_{12}$, corresponding to a π -pulse. In the Ramsey configuration (Figure 10(b)), we maintained the same excitation amplitude but rather than a π -pulse we applied two pulses of excitation, each lasting $\tau_{\text{exc}} = \pi/2\tilde{\Omega}_{12}$ ($\pi/2$ -pulse) separated by a free evolution time $\tau_{\text{free}} = 100$. In both protocols, we successfully transferred the population from the ground state to the quadrupole mode.

Similarly, Figs. 10(c) and (d) illustrate the same process for the breathing mode, with the external frequency adjusted to match the frequency of the breathing mode and the pulses were applied respective to the Rabi-like frequency $\tilde{\Omega}_{13}$. Notably, a rapid frequency component contributes to this dynamics, particularly in the quadrupole case. In a nutshell, this contribution comes from the $e^{i(\omega_{\text{exc}} + \omega_{Q,B})t}$ term which arises when we consider the time evolution of the density operator $\hat{\rho}$ [36]. In this case, since the rotating wave approximation [35, 36] (RWA) was not assumed in the numerical calculations, we end up with this behavior. Typically, the RWA is valid when this term oscillates much faster than the Rabi oscillations, then averaging to zero, as observed in the coherent control of the breathing mode, when each period of the Rabi oscillations takes a considerable time. For the quadrupole mode, however, this term is not so faster than the Rabi oscillations. When this happens in a more significant way, coherent control can be affected; nonetheless, this was not observed for $\lambda = 1/2$. Conversely, for higher values of λ , the influence of non-coherent modes is significant, as discussed before, and the three-level model is not valid. This can be seen in Figure 11 for $\lambda = 2$, where the attempt of total transfer to the quadrupole mode failed. The Rabi frequencies associated with $\lambda = 2$ are relatively high (see Table 1), of the order of the external frequency, and the faster rotation term dominates, thus making the coherent control impossible for the quadrupole case.

To illustrate and validate the success of this model in capturing the population dynamics of the collective modes, we can

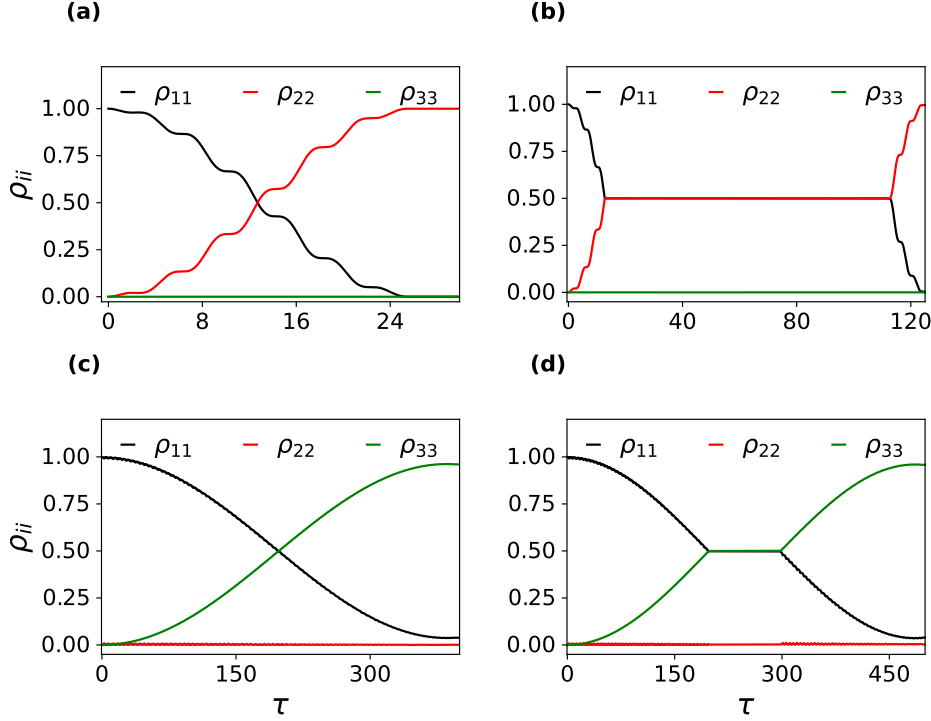


Figure 10: Coherent control of the quadrupole and breathing mode populations for $\lambda = 1/2$ through the application of a π -pulse (panels (a) and (c)) and two $\pi/2$ -pulses (panels (b) and (d)). ρ_{11} , ρ_{22} , and ρ_{33} represent the populations of the ground state, quadrupole mode, and breathing mode, respectively.

apply a π -pulse using the variational method and the Rabi-like frequencies obtained from the three-level model. As discussed earlier, the excitation takes place along the z -axis, aligned with the elongated direction of the BEC, favoring the excitation of the quadrupole mode for configurations with $\lambda < 1$. However, even under these circumstances favoring the quadrupole excitation, when the external frequency is set to be resonant with the breathing transition and a π -pulse $\tau_{\text{exc}} = \pi / \bar{\Omega}_{13}$ is applied, the result is the excitation of the breathing mode.

Figure 12 presents the Fourier transform of the oscillations in the BEC radii when a π -pulse is applied, for $\lambda = 1/2$ and $\lambda = 1$. In contrast to the scenarios presented in Figure 3 for $\lambda = 1/2$ and 1, we observe the breathing mode being practically exclusively excited, showing the successful manipulation of the population in each state.

This outcome suggests the feasibility of coherent control within this system, offering valuable insights for experimentalists investigating specific collective modes. Furthermore, it provides a perspective that collective modes may be interpreted as coherent quantum states, where established concepts from quantum optics can be applied, potentially leading to a description of collective mode dynamics as a macroscopic qubit.

Considering experimental factors such as inherent line broadening in the external excitation, the quadrupole mode might be excited even under conditions intended to excite the breathing mode exclusively. To ensure that most of the population resides in the breathing mode, an additional π -pulse should be implemented, specifically targeting the transition from the quadrupole

to the breathing mode. This process mirrors protocols seen in atomic physics experiments known as repump protocols.

7 CONCLUSIONS

In this work, we explore the coherence properties of a Bose-Einstein condensate (BEC) by employing external pulses inspired by the Rabi and Ramsey protocols to analyze the collective modes of the system. Based on the coherence property of the system, we demonstrate that collective modes can exhibit Ramsey fringes in their resonance curves, allowing for more precise measurements of their resonances when coherence is maintained. This approach enables experimentalists to control the population of collective modes by applying excitation pulses to the system.

We also propose an alternative way to describe the dynamics of collective modes as a system of energy levels, achieving consistent results with those obtained using the variational method. Given the similarities between BECs and coherent radiation fields [46–53], the Ramsey protocol (also known as the separate field technique) [13, 15] holds promise for manipulating quantum states through interference phenomena. Applying this technique to collective modes may advance our understanding of macroscopic quantum systems.

These analyses offer an alternative perspective for observing collective mode dynamics and present a new framework for describing quantum collective modes based on a quantum-level system. A deeper understanding of these properties can provide

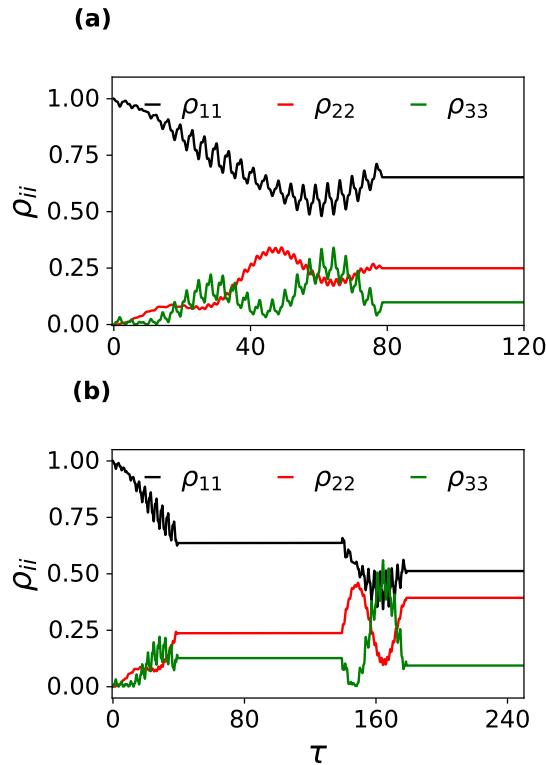


Figure 11: Failed attempt to coherently control the quadrupole population by applying a π -pulse (graph (a)) and by applying two $\pi/2$ -pulses (graphs (b)) for $\lambda = 2$.

insights into the coherence of the system across various regimes of disorder.

8 ACKNOWLEDGMENTS

We thank H. Perrin and R. Dubessy for interesting discussions and valuable insights. This work was supported by the São Paulo Research Foundation (FAPESP) under the grants 2013/07276-1, 2014/50857-8, and 2023/04451-9. L.A.M. acknowledges the support from Coordenação de Aperfeiçoamento de Pessoal de Nível Superior - Brasil (CAPES) - Finance Code 88887.684421/2022-00, 88887.822682/2023-00, and 88887.999663/2024-00. Texas A&M University is acknowledged.

REFERENCES

- [1] A Griffin. The effect of the bose broken symmetry on the dynamics of superfluid 4he: a review. *Canadian Journal of Physics*, 65(11):1368–1376, 1987.
- [2] Franco Dalfovo, Stefano Giorgini, Lev P Pitaevskii, and Sandro Stringari. Theory of bose-einstein condensation in trapped gases. *Reviews of Modern Physics*, 71(3):463, 1999.
- [3] M-O Mewes, MR Andrews, NJ Van Druten, DM Kurn, DS Durfee, CG Townsend, and W Ketterle. Collective excitations of a bose-einstein condensate in a magnetic trap. *Physical Review Letters*, 77(6):988, 1996.
- [4] S. E. Pollack, D. Dries, R. G. Hulet, K. M. F. Magalhães, E. A. L. Henn, E. R. F. Ramos, M. A. Caracanhas, and V. S. Bagnato. Collective excitation of a bose-einstein condensate by modulation of the atomic scattering length. *Physical Review A*, 81:053627, May 2010. doi: 10.1103/PhysRevA.81.053627. URL <https://link.aps.org/doi/10.1103/PhysRevA.81.053627>.
- [5] Guilherme Tomishiyo, Lucas Madeira, and Mônica A Caracanhas. Superfluid excitations in rotating two-dimensional ring traps. *Physics of Fluids*, 36(6), 2024.
- [6] DS Jin, JR Ensher, MR Matthews, CE Wieman, and Eric A Cornell. Collective excitations of a bose-einstein condensate in a dilute gas. *Physical Review Letters*, 77(3):420, 1996.
- [7] F. Dalfovo, C. Minniti, and L. P. Pitaevskii. Frequency shift and mode coupling in the nonlinear dynamics of a bose-condensed gas. *Physical Review A*, 56:4855–4863, Dec 1997. doi: 10.1103/PhysRevA.56.4855. URL <https://link.aps.org/doi/10.1103/PhysRevA.56.4855>.
- [8] Juan J Garcia-Ripoll, Victor M Perez-Garcia, and Pedro Torres. Extended parametric resonances in nonlinear schrödinger systems. *Physical Review Letters*, 83(9):1715, 1999.
- [9] Ivana Vidanović, Antun Balaž, Hamid Al-Jibbouri, and Axel Pelster. Nonlinear bose-einstein-condensate dynamics induced by a harmonic modulation of the s-wave scattering length. *Physical Review A*, 84(1):013618, 2011.
- [10] AR Fritsch, PES Tavares, A Bahrami, YR Tonin, Emanuel Alves de Lima Henn, Vanderlei Salvador Bagnato, and Gustavo Deczka Telles. Nonlinear dependence observed in quadrupolar collective excitation of a trapped bec. *Journal of Low Temperature Physics*, 180:144–152, 2015.
- [11] Isidor Isaac Rabi, Jerrold R Zacharias, Sidney Millman, and Polykarp Kusch. A new method of measuring nuclear magnetic moment. *Physical Review*, 53(4):318, 1938.
- [12] Norman F Ramsey. A molecular beam resonance method with separated oscillating fields. *Physical Review*, 78(6):695, 1950.
- [13] Norman F Ramsey. Experiments with separated oscillatory fields and hydrogen masers. *Reviews of Modern Physics*, 62(3):541, 1990.
- [14] Christopher J Foot. *Atomic physics*, volume 7. OUP Oxford, 2004.
- [15] J Vanier. Atomic clocks based on coherent population trapping: a review. *Applied Physics B*, 81:421–442, 2005.
- [16] Thomas Zanon-Willette, Rémi Lefevre, Rémi Metzдорff, Nicolas Sillitoe, Sylvain Almonacil, Marco Minissale, Emeric De Clercq, Alexey V Taichenachev, Valeriy I Yudin, and Ennio Arimondo. Composite laser-pulses spectroscopy for high-accuracy optical clocks: a review of recent progress and perspectives. *Reports on Progress in Physics*, 81(9):094401, 2018.
- [17] Ch J Bordé, Ch Salomon, S Avrillier, A Van Lerberghe, Ch Bréant, D Bassi, and G Scoles. Optical ramsey fringes

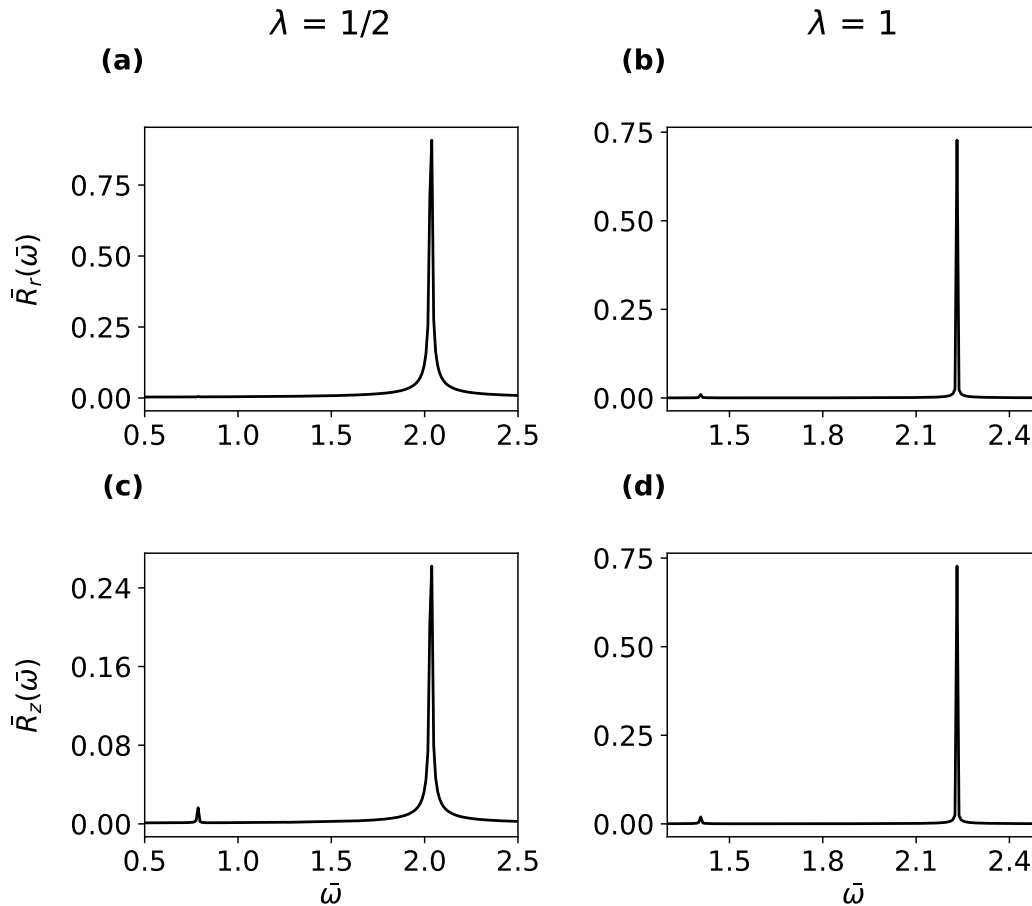


Figure 12: Fourier spectrum obtained from the variational model for $\lambda = 1/2$ (graph (a) and (b)) and for $\lambda = 1$ (graphs (c) and (d)) when a Rabi pulse with duration of $\tau_{\text{exc}} = \pi/\bar{\Omega}_{13}$ is applied. The used Rabi frequency was obtained using the three-level model.

with traveling waves. *Physical Review A*, 30(4):1836, 1984.

- [18] Christopher J Pethick and Henrik Smith. *Bose–Einstein condensation in dilute gases*. Cambridge university press, 2008.
- [19] EAL Henn, JA Seman, GB Seco, EP Olimpio, P Castilho, G Roati, Daniel Varela Magalhães, Kílvia Mayre Farias Magalhães, and Vanderlei Salvador Bagnato. Bose-einstein condensation in 87rb: Characterization of the brazilian experiment. *Brazilian Journal of Physics*, 38:279–286, 2008.
- [20] EAL Henn, JA Seman, ERF Ramos, M Caracanhas, P Castilho, EP Olímpio, G Roati, Daniel Varela Magalhães, Kílvia Mayre Farias Magalhães, and Vanderlei Salvador Bagnato. Observation of vortex formation in an oscillating trapped bose-einstein condensate. *Physical Review A*, 79(4):043618, 2009.
- [21] AD García-Orozco, Lucas Madeira, MA Moreno-Armijos, Amilson Rogesio Fritsch, Pedro Ernesto Schiavinatti Tavares, Patricia Christina Marques Castilho, André Cidrim, G Roati, and Vanderlei Salvador Bagnato. Universal dynamics of a turbulent superfluid bose gas. *Physical Review A*, 106(2):023314, 2022.
- [22] M Desaix, D Anderson, and M Lisak. Variational approach to collapse of optical pulses. *JOSA B*, 8(10):2082–2086, 1991.
- [23] Victor M Perez-Garcia, Humberto Michinel, JI Cirac, M Lewenstein, and P Zoller. Low energy excitations of a bose-einstein condensate: A time-dependent variational analysis. *Physical Review Letters*, 77(27):5320, 1996.
- [24] ERF Ramos, FEA Dos Santos, Mônica Andrioli Caracanhas, and Vanderlei Salvador Bagnato. Coupling collective modes in a trapped superfluid. *Physical Review A*, 85(3):033608, 2012.
- [25] Y Castin and R Dum. Bose-einstein condensates in time dependent traps. *Physical Review Letters*, 77(27):5315, 1996.
- [26] Huang Guo-Xiang. Second harmonic generation of propagating collective excitations in bose–einstein condensates. *Chinese Physics*, 13(11):1866, 2004.
- [27] G Hechenblaikner, OM Marago, E Hodby, J Arlt, S Hopkins, and CJ Foot. Observation of harmonic generation

- and nonlinear coupling in the collective dynamics of a bose-einstein condensate. *Physical Review Letters*, 85(4): 692, 2000.
- [28] Paul J Campagnola, Aaron Lewis, Leslie M Loew, et al. High-resolution nonlinear optical imaging of live cells by second harmonic generation. *Biophysical Journal*, 77(6): 3341–3349, 1999.
- [29] Vanderlei S Bagnato, Rashid G Nazmitdinov, and Vyacheslav I Yukalov. Symmetry in many-body physics, 2022.
- [30] Onofrio Marago, Gerald Hechenblaikner, Eleanor Hodby, and Christopher Foot. Temperature dependence of damping and frequency shifts of the scissors mode of a trapped bose-einstein condensate. *Physical Review Letters*, 86(18): 3938, 2001.
- [31] Yu Zhou, Wen Wen, and Guoxiang Huang. Frequency shift and mode coupling of the collective modes of superfluid fermi gases in the bcs-bec crossover. *Physical Review B—Condensed Matter and Materials Physics*, 77(10):104527, 2008.
- [32] DS Jin, MR Matthews, JR Ensher, CE Wieman, and Eric A Cornell. Temperature-dependent damping and frequency shifts in collective excitations of a dilute bose-einstein condensate. *Physical Review Letters*, 78(5):764, 1997.
- [33] Masahito Ueda. *Fundamentals and new frontiers of Bose-Einstein condensation*. World Scientific, 2010.
- [34] Jun John Sakurai and Jim Napolitano. *Modern quantum mechanics*. Cambridge University Press, 2020.
- [35] Heinz-Peter Breuer and Francesco Petruccione. *The theory of open quantum systems*. Oxford University Press, USA, 2002.
- [36] Michael A Nielsen and Isaac L Chuang. *Quantum computation and quantum information*. Cambridge university press, 2010.
- [37] Marc E Songolo and Brigitte Bidégaray-Fesquet. Non-standard finite-difference schemes for the two-level bloch model. *International Journal of Modeling, Simulation, and Scientific Computing*, 9(04):1850033, 2018.
- [38] Marc E Songolo and Brigitte Bidégaray-Fesquet. Strang splitting schemes for n-level bloch models. *International Journal of Modeling, Simulation, and Scientific Computing*, page 2350044, 2023.
- [39] NR Draper. *Applied regression analysis*. McGraw-Hill. Inc, 1998.
- [40] Sergey N Shevchenko, Sahel Ashhab, and Franco Nori. Landau–zener–stückelberg interferometry. *Physics Reports*, 492(1):1–30, 2010.
- [41] Curt Wittig. The landau- zener formula. *The Journal of Physical Chemistry B*, 109(17):8428–8430, 2005.
- [42] Yaron Silberberg. Quantum coherent control for nonlinear spectroscopy and microscopy. *Annual Review of Physical Chemistry*, 60:277–292, 2009.
- [43] U Sterr, K Sengstock, JH Müller, D Bettermann, and W Ertmer. The magnesium ramsey interferometer: Applications and prospects. *Applied Physics B*, 54:341–346, 1992.
- [44] Patrice Bertet, S Osnaghi, A Rauschenbeutel, G Nogues, A Auffeves, M Brune, JM Raimond, and S Haroche. A complementarity experiment with an interferometer at the quantum–classical boundary. *Nature*, 411(6834):166–170, 2001.
- [45] C Wan, M Scala, GW Morley, ATM A Rahman, Hendrik Ulbricht, James Bateman, PF Barker, Sougato Bose, and MS Kim. Free nano-object ramsey interferometry for large quantum superpositions. *Physical Review Letters*, 117(14): 143003, 2016.
- [46] MR Andrews, CG Townsend, H-J Miesner, DS Durfee, DM Kurn, and W Ketterle. Observation of interference between two bose condensates. *Science*, 275(5300):637–641, 1997.
- [47] M-O Mewes, MR Andrews, DM Kurn, DS Durfee, CG Townsend, and W Ketterle. Output coupler for bose-einstein condensed atoms. *Physical Review Letters*, 78(4): 582, 1997.
- [48] Immanuel Bloch, Theodor W Hänsch, and Tilman Esslinger. Atom laser with a cw output coupler. *Physical Review Letters*, 82(15):3008, 1999.
- [49] FRANCESCO SAVERIO Cataliotti, Sven Burger, Chiara Fort, P Maddaloni, Francesco Minardi, Andrea Trombettoni, Augusto Smerzi, and Massimo Inguscio. Josephson junction arrays with bose-einstein condensates. *Science*, 293(5531):843–846, 2001.
- [50] F Dalfovo, L Pitaevskii, and S Stringari. Order parameter at the boundary of a trapped bose gas. *Physical Review A*, 54(5):4213, 1996.
- [51] Pedro ES Tavares, Amilson R Fritsch, Gustavo D Telles, Mahir S Hussein, François Impens, Robin Kaiser, and Vanderlei S Bagnato. Matter wave speckle observed in an out-of-equilibrium quantum fluid. *Proceedings of the National Academy of Sciences*, 114(48):12691–12695, 2017.
- [52] Lucas Madeira and Vanderlei S Bagnato. Cold atoms beyond atomic physics. *Brazilian Journal of Physics*, 51(2):170–180, 2021.
- [53] Giovanni Modugno. Anderson localization in bose-einstein condensates. *Reports on Progress in Physics*, 73(10):102401, 2010.